M&C 2017 - International Conference on Mathematics & Computational Methods Applied to Nuclear Science & Engineering, Jeju, Korea, April 16-20, 2017, on USB (2017)

Inverse Estimation of Unknown Radioactive Source using Detection Probability and Adjoint Calculation

Shinji SUGAYA, Tomohiro ENDO, Akio YAMAMOTO

Nagoya University: Furo-cho, Chikusa-ku, Nagoya, Japan, 464-8603
s-sugaya@fermi.nucl.nagoya-u.ac.jp, t-endo@nucl.nagoya-u.ac.jp, a-yamamoto@nucl.nagoya-u.ac.jp

Abstract - *In order to investigate distribution of fuel debris remaining in the reactor containment vessel of Fukushima Daiichi NPS, we focused on the estimations based on the measured value of neutron counts. Maximum Likelihood-Expectation Maximization (ML-EM) method and Moore-Penrose Matrix Inverse (MPMI) method were examined. The ML-EM method is used for image reconstruction of Computed Tomography, and the MPMI method is one of the solution of the simultaneous linear equations. Concrete shielding were set between detectors and neutron sources in the calculation system, since where detector position in actual applications would be outside of the shielding such as the pedestal. Since sufficient number of count measurement positions would not be secured owing to the complexity of structures inside containment vessel, the number of measurement points were set to be smaller than that of neutron sources. Since the detection probability is used as the coupling coefficient between the radiation count and the radioactivity, the adjoint transport calculation is performed to obtain the detection probability. The detection probability calculated by adjoint neutron flux reproduced the physical trend expected from detector and neutron source positions. Result of estimation using this detection probability indicates that two methods gave reasonable neutron emission rate distribution that is close to the true value.*

I. INTRODUCTION

In Fukushima Daiichi Nuclear Power Plant (1F), decommissioning of the nuclear reactors experienced severe accident is being carried out. The retrieval of fuel debris remaining in the reactor pressure vessel and/or the containment vessel (RPV/CV) is expected one of the most difficult works since we have few experience in the past. Information on the distribution of fuel debris in RPV/CV is essential to establish a roadmap plan to remove it, to prevent unexpected re-critical accident during removal works and to determine shielding of radiation from fuel debris during and after removal. Especially the risk of re-criticality of fuel by taking actions to the system is studied in Ref.[1] etc., and it is one of the issues in the removal of fuel debris.

Removal strategy of fuel debris of 1F Unit 1 is going to be established in the first half of 2018 and the detail information inside RPV/CV is highly desirable. Investigation using muon suggests that most of fuel debris would not resident in RPV in Unit 1. Contrary, in Unit 2, most of fuel debris would still exist at the RPV bottom head. However, more detail estimation on location of fuel debris is desirable. Location identification of fuel debris is being tried, e.g. Ref.[2], but improvement of reliability on prediction results is necessary using various methods.

In this study, we try to estimate distribution of radioactive sources using multiple measurement results of radiation and inverse analysis methods, i.e. the Maximum Likelihood–Expectation Maximization (ML-EM) method and the Moore-Penrose Matrix Inverse (MPMI) method. In these inverse analysis methods, detection probability of radiation emitted from a radioactive source is necessary. Though various approaches can be used to evaluate the detection probability, a numerical transport calculation using the discrete ordinate method is adopted. A simplified calculation model simulating pedestal and shielding around RPV is constructed and used for analysis. Through verification calculations, effectiveness and validity of the present method is confirmed.

II. THEORY

Structures inside RPV/CV are complicated as well as distribution of fuel debris. On the other hand, measurement points of radiation inside RPV/CV are very limited. Therefore, the inverse problem of this study should treat an underdetermined system, where the number of unknowns (radioactivity) is larger than that of constraint conditions (radiation measurement results by detectors). There are some techniques to estimate a plausible solution for such an inverse problem. In this study, we use the following two methods: One is Maximum Likelihood-Expectation Maximization (ML-EM) method; another is Moore-Penrose Matrix Inverse (MPMI) method. Let us assume that radioactive sources are point-sources emitting neutrons and estimate the neutron emission rate at each source-position. In this case, the three-dimensional distribution of radioactive intensity of point sources can be estimated using these two methods.

1. Maximum Likelihood-Expectation Maximization (ML-EM) method

The ML-EM method is one of the techniques based on the Bayesian estimation. In the image reconstruction of Computed Tomography (CT), the ML-EM method is effectively utilized [3,4]. The inverse problem of this study is similar to that of CT, thus we try applying the ML-EM

method to estimate radioactivity distribution. The radioactivity can be estimated by considering a prior radioactivity distribution A_j and measured values of radiation count y_i. Using the iterative calculation of Eq. (1), the converged solution of radioactivity can be finally obtained:

$$A_j^{k+1} = \frac{A_j^k}{\sum_{i=1}^{I} C_{ij}} \sum_{i=i}^{I} \frac{y_i C_{ij}}{\sum_{j=1}^{J} C_{ij} A_j^k}. \quad (1)$$

Detailed derivation of Eq. (1) is described as follows. x_{ij} indicates the number of radiations emitted from the radiation source j and detected by the detector i. x_{ij} obeys the Poisson distribution and can be regarded as independent. Therefore, the occurrence probability of the event, which the radiation count becomes $(x_{11}, x_{12}, \dots, x_{1J}, x_{21}, x_{22}, \dots, x_{2J}, \dots, x_{IJ})$, is expressed by Eq. (2):

$$P(\boldsymbol{x}_{I,J}) = \prod_{i=1}^{I}\prod_{j=1}^{J} e^{-\overline{x_{ij}}} \frac{\overline{x_{ij}}^{x_{ij}}}{x_{ij}!} = \prod_{i=1}^{I}\prod_{j=1}^{J} e^{-C_{ij}A_j} \frac{(C_{ij}A_j)^{x_{ij}}}{x_{ij}!}. \quad (2)$$

It should be noted that the relation $\overline{x_{ij}} = C_{ij}A_j$ is used.

We try to find the values of A_j that give the maximum value of the probability expressed by Eq. (2). At first, we take the logarithm of Eq. (2) as shown in Eq. (3). Then Eq. (3) is diffentiated by A_j. Since the logarithmic function increases monotonically and A_j is positive, the values of A_j obtained by partial diffentiation of Eq. (3) also gives the maximum value for Eq. (2).

$$\ln\left(P(\boldsymbol{x}_{I,J})\right) = \sum_{i=1}^{I}\sum_{j=1}^{J}\left(-C_{ij}A_j + x_{ij}(\ln C_{ij} + \ln A_j) - \ln(x_{ij}!)\right) = \sum_{i=1}^{I}\sum_{j=1}^{J}(-C_{ij}A_j + x_{ij}\ln A_j) + c = L. \quad (3)$$

The term which does not depend on A_j is replaced by c. In addition, L is used for simplification. Since x_{ij} is not known in actual measurement, $E[x_{ij}|y_i]$, which is the expected value of x_{ij} when y_i is given, is used. Then Eq. (3) also changes to the expression of expected value as shown in Eq. (4):

$$E[L|\vec{y}] = \sum_{i=1}^{I}\sum_{j=1}^{J}(-C_{ij}A_j + E[x_{ij}|y_i]\ln A_j) + c. \quad (4)$$

To obtain the expression of $E[x_{ij}|y_i]$, we consider $P(x_{ij}|y_i)$, which is the conditional probability of x_{ij} when y_i is given. $P(x_{ij}|y_i)$ is expressed by Eq. (5) from the Bayesian formula:

$$P(x_{ij}|y_i) = \frac{P(x_{ij})P(y_i|x_{ij})}{P(y_i)}. \quad (5)$$

$P(y_i|x_{ij})$ is the probability that the radiation count is y_i under the condition off given x_{ij}. Therefore $P(y_i|x_{ij})$ is expressed by Eq. (6):

$$P(y_i|x_{ij}) = P(y_i - x_{ij}) = e^{-(\sum_{m=1}^{J} C_{im}A_m - C_{ij}A_j)} \frac{(\sum_{m=1}^{J} C_{im}A_m - C_{ij}A_j)^{y_i - x_{ij}}}{(y_i - x_{ij})!}. \quad (6)$$

Note that the relations of $y_i = \sum_{m=1}^{J} C_{im}A_m$ and $x_{ij} = C_{ij}A_j$ are used. Then, $P(x_{ij}|y_i)$ in Eq. (5) can be written as:

$$\begin{aligned} P(x_{ij}|y_i) &= \frac{e^{-C_{ij}A_j}\frac{(C_{ij}A_j)^{x_{ij}}}{x_{ij}!} e^{-(\sum_{m=1}^{J} C_{im}A_m - C_{ij}A_j)} \frac{(\sum_{m=1}^{J} C_{im}A_m - C_{ij}A_j)^{y_i - x_{ij}}}{(y_i - x_{ij})!}}{e^{-\sum_{j=1}^{J} C_{ij}A_j} \frac{\left(\sum_{j=1}^{J} C_{ij}A_j\right)^{y_i}}{y_i!}} \\ &= {}_{y_i}C_{x_{ij}} \frac{e^{-C_{ij}A_j} e^{-(\sum_{m=1}^{J} C_{im}A_m - C_{ij}A_j)}}{e^{-\sum_{j=1}^{J} C_{ij}A_j}} \frac{(C_{ij}A_j)^{x_{ij}} (\sum_{m=1}^{J} C_{im}A_m - C_{ij}A_j)^{y_i - x_{ij}}}{\left(\sum_{j=1}^{J} C_{ij}A_j\right)^{y_i}} \\ &= {}_{y_i}C_{x_{ij}} \times 1 \times \frac{(C_{ij}A_j)^{x_{ij}} (\sum_{m=1}^{J} C_{im}A_m - C_{ij}A_j)^{y_i - x_{ij}}}{\left(\sum_{j=1}^{J} C_{ij}A_j\right)^{x_{ij}} \left(\sum_{j=1}^{J} C_{ij}A_j\right)^{-x_{ij}} \left(\sum_{j=1}^{J} C_{ij}A_j\right)^{y_i}} \\ &= {}_{y_i}C_{x_{ij}} \left(\frac{C_{ij}A_j}{\sum_{j=1}^{J} C_{ij}A_j}\right)^{x_{ij}} \left(\frac{\sum_{m=1}^{J} C_{im}A_m - C_{ij}A_j}{\sum_{j=1}^{J} C_{ij}A_j}\right)^{y_i - x_{ij}} \\ &= {}_{y_i}C_{x_{ij}} \left(\frac{C_{ij}A_j}{\sum_{j=1}^{J} C_{ij}A_j}\right)^{x_{ij}} \left(1 - \frac{C_{ij}A_j}{\sum_{j=1}^{J} C_{ij}A_j}\right)^{y_i - x_{ij}}. \end{aligned} \quad (7)$$

Note that ${}_{k}C_{l}$ indicates number of combinations.

Equation (7) is interpreted as the probability distribution of trials where the number of trials is y_i, the success count is x_{ij}, and the success probability is $\frac{C_{ij}A_j}{\sum_{j=1}^{J} C_{ij}A_j}$. $E[x_{ij}|y_i]$ is expressed by Eq. (8) since (Expected value of success count) = (number of trials) × (success probability):

$$E[x_{ij}|y_i] = y_i \frac{C_{ij}A_j}{\sum_{j=1}^{J} C_{ij}A_j}. \quad (8)$$

We substitute Eq. (8) into Eq. (4) and find the value of A_j which satisfies the value of partial differential equation of Eq. (4) to be zero, as shown in Eq. (9). Instead of A_j, we use A_j^k obtained in k-th iteration calculation.

$$\frac{\partial}{\partial A_j} E[\mathrm{L}|\vec{y}, \vec{A}^k] = 0 \quad (9)$$

$$\frac{\partial}{\partial A_j}\left[\sum_{i=1}^{I}\sum_{j=1}^{J}\left(-C_{ij}A_j+\frac{y_i C_{ij}A_j^k}{\sum_{j=1}^{J}C_{ij}A_j^k}\ln A_j\right)+c\right]$$
$$=\sum_{i=1}^{I}\left(-C_{ij}+\frac{y_i C_{ij}A_j^k}{\sum_{j=1}^{J}C_{ij}A_j^k}\frac{1}{A_j}\right)$$
$$=-\sum_{i=1}^{I}C_{ij}+\frac{1}{A_j}\sum_{i=1}^{I}\frac{y_i C_{ij}A_j^k}{\sum_{j=1}^{J}C_{ij}A_j^k}$$
$$=0$$

$$\widehat{A_j}=\frac{1}{\sum_{i=1}^{I}C_{ij}}\sum_{i=1}^{I}\frac{y_i C_{ij}A_j^k}{\sum_{j=1}^{J}C_{ij}A_j^k}=\frac{A_j^k}{\sum_{i=1}^{I}C_{ij}}\sum_{i=1}^{I}\frac{y_i C_{ij}}{\sum_{j=1}^{J}C_{ij}A_j^k}.$$

By setting $\widehat{A_j}$ as A_j^{k+1}, which is the updated value of A_j^k, Eq. (1) can be obtained.

2. Moore-Penrose Matrix Inverse (MPMI) method

The inverse problem of radioactivity in this study can be expressed by the following simultaneous linear equations:

$$\mathbf{C}\vec{A}\approx\vec{y}, \tag{10}$$

where $\mathbf{C}$ is a $I\times J$ matrix of detection probability. For example, Eq. (10) is rewritten by Eq. (11) when the numbers of detectors and radioactive sources are 2 and 3, respectively:

$$\begin{pmatrix}C_{11} & C_{12} & C_{13}\\ C_{21} & C_{22} & C_{23}\end{pmatrix}\begin{pmatrix}A_1\\A_2\\A_3\end{pmatrix}\approx\begin{pmatrix}y_1\\y_2\end{pmatrix}. \tag{11}$$

Figure 1 is shown as a diagram of this situation.

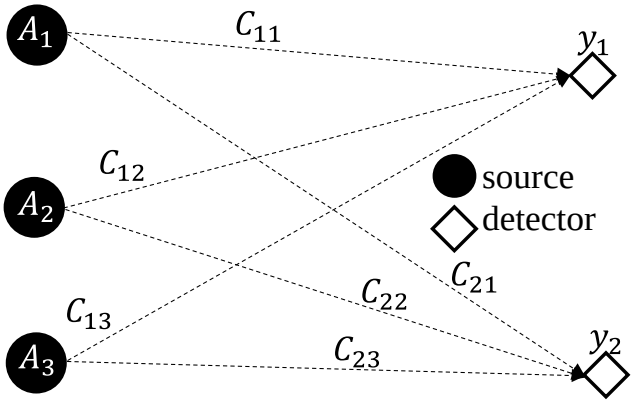

Fig. 1 Three neutron sources and two detectors

Simultaneous linear equations of an underdetermined system cannot be solved by a normal inverse matrix. Even in this case, a minimum L2-norm solution $\vec{A}_{MPMI}$ can be numerically solved using MPMI, i.e.

$$\vec{A}_{MPMI}=\begin{pmatrix}C_{11} & C_{12} & C_{13}\\ C_{21} & C_{22} & C_{23}\end{pmatrix}^{+}\begin{pmatrix}y_1\\y_2\end{pmatrix}, \tag{12}$$

where the superscript + means the Moore-Penrose pseudoinverse. The condition that L2-norm is minimum is necessary to uniquely obtain the solution of $\vec{A}$ for the underdetermined system. For example, when the numbers of constraint conditions and unknowns are respectively 2 and 3, all solutions of (A_1, A_2, A_3) satisfying Eq. (10) correspond to arbitrary points on the plane-plane intersection: $C_{11}A_1+C_{12}A_2+C_{13}A_3=y_1$ and $C_{21}A_1+C_{22}A_2+C_{23}A_3=y_2$. The minimum L2-norm solution $(A_{MP,1}, A_{MP,2}, A_{MP,3})$ corresponds to the nearest point from the origin $(0,0,0)$.

In order to numerically solve $\vec{A}_{MPMI}$, the singular value decomposition is used. We can perform singular value decomposition by using proper matrices of $\mathbf{U}, \mathbf{V}$ and singular values of $\mathbf{C}$:

$$\mathbf{C}=\mathbf{U}\mathbf{\Sigma}\mathbf{V}^{\mathrm{T}}=\mathbf{U}\begin{pmatrix}\mathrm{diag}(\sigma_1,\dots,\sigma_r) & \mathbf{0}_{r,J-r}\\ \mathbf{0}_{I-r,r} & \mathbf{0}_{I-r,J-r}\end{pmatrix}\mathbf{V}^{\mathrm{T}}. \tag{13}$$

First, we find $\vec{A}$ satisfying Eq. (10). That is, we aim to find $\vec{A}$ satisfying $\left\|\mathbf{C}\vec{A}-\vec{y}\right\|^2=0$. By using the property of the orthogonal matrix, Eq. (14) can be obtained:

$$\begin{aligned}\left\|\mathbf{C}\vec{A}-\vec{y}\right\|^2&=\left(\mathbf{C}\vec{A}-\vec{y}\right)^{\mathrm{T}}\left(\mathbf{C}\vec{A}-\vec{y}\right)\\&=\left\{\mathbf{U}\left(\mathbf{\Sigma}\mathbf{V}^{\mathrm{T}}\vec{A}-\mathbf{U}^{\mathrm{T}}\vec{y}\right)\right\}^{\mathrm{T}}\mathbf{U}\left(\mathbf{\Sigma}\mathbf{V}^{\mathrm{T}}\vec{A}-\mathbf{U}^{\mathrm{T}}\vec{y}\right)\\&=\left(\mathbf{\Sigma}\mathbf{V}^{\mathrm{T}}\vec{A}-\mathbf{U}^{\mathrm{T}}\vec{y}\right)^{\mathrm{T}}\mathbf{U}^{\mathrm{T}}\mathbf{U}\left(\mathbf{\Sigma}\mathbf{V}^{\mathrm{T}}\vec{A}-\mathbf{U}^{\mathrm{T}}\vec{y}\right)\\&=\left(\mathbf{\Sigma}\mathbf{V}^{\mathrm{T}}\vec{A}-\mathbf{U}^{\mathrm{T}}\vec{y}\right)^{T}\left(\mathbf{\Sigma}\mathbf{V}^{\mathrm{T}}\vec{A}-\mathbf{U}^{\mathrm{T}}\vec{y}\right)\\&=\left\|\mathbf{\Sigma}\mathbf{V}^{\mathrm{T}}\vec{A}-\mathbf{U}^{\mathrm{T}}\vec{y}\right\|^2.\end{aligned} \tag{14}$$

Replacing $\mathbf{V}^{\mathrm{T}}\vec{A}$ with $\vec{x}$ and $\mathbf{U}^{\mathrm{T}}\vec{y}$ with $\vec{b}$, $\left\|\mathbf{\Sigma}\mathbf{V}^{\mathrm{T}}\vec{A}-\mathbf{U}^{\mathrm{T}}\vec{y}\right\|^2$ is expressed by Eq. (15):

$$\left\|\mathbf{\Sigma}\vec{x}-\vec{b}\right\|^2=\sum_{i=1}^{r}(\sigma_i x_i-b_i)^2+\sum_{i=r+1}^{I}{b_i}^2. \tag{15}$$

Here, the second term of in the right hand of Eq. (15) can be regarded as 0 for considering the situation of underdetermined system: $r=I$. Therefore, by using $\vec{x}$ of Eq. (16), we make the first term of Eq. (15) to be zero. $\vec{d}$ is any vector with $(J-I)$ elements.

$$\vec{x}=\begin{pmatrix}b_1{\sigma_1}^{-1}\\ \vdots\\ b_I{\sigma_I}^{-1}\\ \vec{d}\end{pmatrix}=\begin{pmatrix}\mathrm{diag}({\sigma_1}^{-1},\dots,{\sigma_I}^{-1})\,\vec{b}\\ \vec{d}\end{pmatrix}. \tag{16}$$

Then $\vec{A}$ is given by Eq. (17):

$$\vec{A} = \mathbf{V}\mathbf{V}^{\mathrm{T}}\vec{A} = \mathbf{V}\vec{x} = \mathbf{V}\begin{pmatrix}\mathrm{diag}({\sigma_1}^{-1}, \dots, {\sigma_I}^{-1})\,\vec{b}\\ \vec{d}\end{pmatrix}. \quad (17)$$

$\vec{A}$ with $\vec{d} = 0$, whose L2-norm is minimum within the solution of Eq. (10), i.e. $\vec{A}_{MPMI}$ is expressed by Eq. (18).

$$\begin{aligned}\vec{A}_{MPMI} &= \mathbf{V}\begin{pmatrix}\mathrm{diag}({\sigma_1}^{-1}, \dots, {\sigma_I}^{-1})\,\mathbf{U}^{\mathrm{T}}\vec{y}\\ \mathbf{0}_{J-I}\end{pmatrix}\\ &= \left(\mathbf{V}\begin{pmatrix}\mathrm{diag}({\sigma_1}^{-1}, \dots, {\sigma_I}^{-1})\\ \mathbf{0}_{J-I}\end{pmatrix}\mathbf{U}^{\mathrm{T}}\right)\vec{y} = \mathbf{C}^{+}\vec{y}.\end{aligned} \quad (18)$$

III. CALCULATION OF DETECTION PROBABILITY

In this section, a calculation method of detection probability C_{ij} is described [5]. The stationary neutron transport equation with the external neutron source is given by Eqs. (19)-(21):

$$\mathbf{A}\psi(\vec{r}, E, \vec{\Omega}) = \mathbf{F}\psi(\vec{r}, E, \vec{\Omega}) + \frac{S(\vec{r}, E)}{4\pi}, \quad (19)$$

$$\begin{aligned}\mathbf{A} \equiv \vec{\Omega}\nabla + \Sigma_{\mathrm{t}}(\vec{r}, E) - \int_0^{\infty} dE' \int_{4\pi} d\vec{\Omega}\,\Sigma_{\mathrm{s}}(\vec{r}, E'\\ \to E, \vec{\Omega}' \to \vec{\Omega}),\end{aligned} \quad (20)$$

$$\mathbf{F} \equiv \frac{\chi(\vec{r}, E)}{4\pi}\int_0^{\infty} dE' \int_{4\pi} d\vec{\Omega}\,\nu\Sigma_{\mathrm{f}}(\vec{r}, E'). \quad (21)$$

The adjoint neutron transport equation corresponding to Eqs. (19)-(21) is given in Eqs. (22)-(24):

$$\mathbf{A}^{\dagger}\psi^{\dagger} = \mathbf{F}^{\dagger}\psi^{\dagger} + \frac{\Sigma_{\mathrm{d,i}}(\vec{r}, E)}{4\pi}, \quad (22)$$

$$\begin{aligned}\mathbf{A}^{\dagger} \equiv -\vec{\Omega}\nabla + \Sigma_{\mathrm{t}}(\vec{r}, E) - \int_0^{\infty} dE' \int_{4\pi} d\vec{\Omega}'\,\Sigma_{\mathrm{s}}(\vec{r}, E\\ \to E', \vec{\Omega} \to \vec{\Omega}'),\end{aligned} \quad (23)$$

$$\mathbf{F}^{\dagger} \equiv \nu\Sigma_{\mathrm{f}}(\vec{r}, E)\int_0^{\infty} dE' \int_{4\pi} d\vec{\Omega}'\frac{\chi(\vec{r}, E')}{4\pi}. \quad (24)$$

$\mathbf{A}^{\dagger}$ and $\mathbf{F}^{\dagger}$ are the adjoint operators corresponding to **A** and **F**, respectively. Equation (25) is obtained by multiplying both sides of Eq. (19) by $\psi^{\dagger}$ from the left side and integrating in all phase space: $\vec{r}, E, \vec{\Omega}$.

$$\langle\psi^{\dagger}\mathbf{A}\psi\rangle = \langle\psi^{\dagger}\mathbf{F}\psi\rangle + \langle\psi^{\dagger}\frac{S}{4\pi}\rangle. \quad (25)$$

The adjoint neutron source is represented by the symbol of the detection cross section. With similar procedure for Eq. (22), Eq. (26) is also obtained:

$$\langle\psi\mathbf{A}^{\dagger}\psi^{\dagger}\rangle = \langle\psi\mathbf{F}^{\dagger}\psi^{\dagger}\rangle + \langle\psi\frac{\Sigma_{\mathrm{d,i}}}{4\pi}\rangle. \quad (26)$$

On the other hand, from the property of adjoint operator, Eqs. (27) and (28) are established:

$$\langle\psi^{\dagger}\mathbf{A}\psi\rangle = \langle\psi\mathbf{A}^{\dagger}\psi^{\dagger}\rangle, \quad (27)$$

$$\langle\psi^{\dagger}\mathbf{F}\psi\rangle = \langle\psi\mathbf{F}^{\dagger}\psi^{\dagger}\rangle. \quad (28)$$

Equation (29) can be derived from the Eqs. (25)-(28):

$$\begin{aligned}&\langle\psi^{\dagger}\frac{S}{4\pi}\rangle = \langle\psi\frac{\Sigma_{\mathrm{d,i}}}{4\pi}\rangle\\ &\int_V dV\int_0^{\infty} dE\int_{4\pi} d\vec{\Omega}\,S(\vec{r}, E)\psi^{\dagger}(\vec{r}, E, \vec{\Omega})\\ &= \int_V dV\int_0^{\infty} dE\int_{4\pi} d\vec{\Omega}\,\Sigma_{\mathrm{d,i}}(\vec{r}, E)\psi(\vec{r}, E, \vec{\Omega}),\end{aligned} \quad (29)$$

Point neutron source S at $\vec{r}_j$ is expressed by Eq. (30). S can be regarded as the spontaneous fission source the situation considered in the present study.

$$\begin{aligned}&S(\vec{r}, E)\\ &= (\text{neutron emisson rate at position } \vec{r}_j)\\ &\times \delta(\vec{r} - \vec{r}_j)\chi(E).\end{aligned} \quad (30)$$

Using Eq. (30), we can obtain C_{ij} as:

$$\begin{aligned}&(\text{neutron emisson rate at position } \vec{r}_j)\\ &\times\int_0^{\infty} dE\int_{4\pi} d\vec{\Omega}\,\chi(E)\psi^{\dagger}(\vec{r}_j, E, \vec{\Omega})\\ &= \int_V dV\int_0^{\infty} dE\int_{4\pi} d\vec{\Omega}\,\Sigma_{\mathrm{d,i}}(\vec{r}, E)\psi(\vec{r}, E, \vec{\Omega})\\ &= (\text{neutron count rate at position } \vec{r}_j)\\ &\int_0^{\infty} dE\,\chi(E)\phi^{\dagger}(\vec{r}_j, E, \vec{\Omega})\\ &= \frac{(\text{neutron count rate at detector } i)}{(\text{neutron emisson rate at position } \vec{r}_j)} = C_{ij}.\end{aligned} \quad (31)$$

It should be noted that neutron multiplication is not considered in the present study.

IV. CALCULATION PROCEDURE

As a simple problem, let us consider an annular concrete shielding as shown in Fig. 2. Other regions except for the shielding are void. All boundary conditions are vacuum conditions. Two ring-detectors ($i = 1,2$) and three point-sources ($j = 1,2,3$) are considered in this geometry. The calculation conditions of detectors and neutron sources are summarized in Tables I and II. In this calculation, the thermal detection cross-section $\Sigma_{\mathrm{d},1}$ is zero. Since majorneutron source is spontaneous fission, source strength of thermal neutron S_2 is assumed to be zero.

Table I Calculation condition; neutron detectors

i	r[cm]	z[cm]	Σ_{d1}, Σ_{d2}[1/cm]	
1	599-600	96-100	0	0.01
2	599-600	596-600	0	0.01

Table II Calculation condition; neutron sources

j	r[cm]	z[cm]	S_1, S_2[neutrons/sec]	
1	0	0	9.00E+13	0
2	0	200	5.00E+13	0
3	0	400	1.00E+13	0

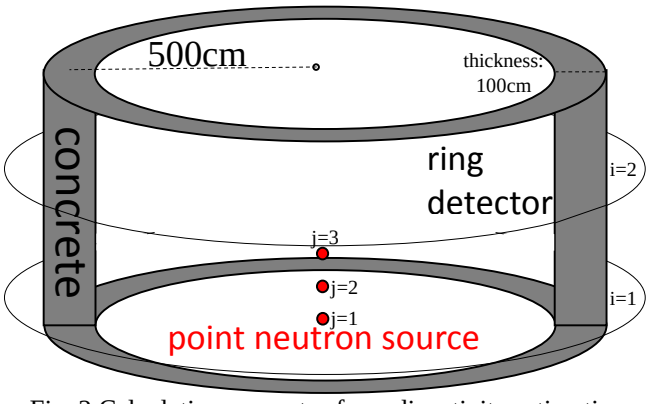

Fig. 2 Calculation geometry for radioactivity estimation

Before calculation of the detection probability C_{ij} (detection probability of a neutron at each detector i emitted from source j) in the calculation geometry of Fig. 2, we prepared two group macroscopic cross-section for concrete using SCALE6.2.1/NEWT [6]. The energy boundary between fast and thermal energy is 0.625 [eV]. The two group cross-sections were collapsed using neutron spectrum obtained by a forward transport calculation of NEWT in Fig. 3, where fuel region of UO_2 was used to obtain a typical neutron flux spectrum in concrete. Thickness of concrete wall in Fig. 3 is set based on Fig. 2. In Fig. 3, the left and right boundary conditions are vacuum; and upper and lower ones are periodic, respectively.

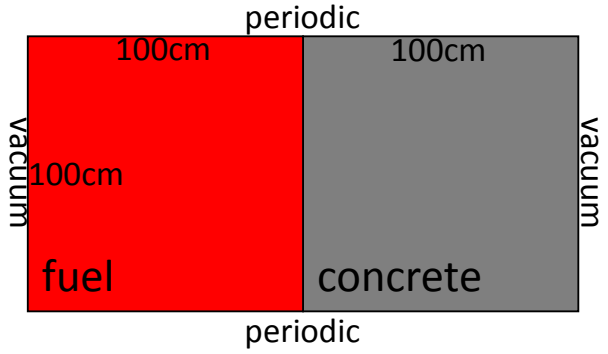

Fig. 3 Calculation geometry of NEWT to obtain two-group macroscopic cross-section of concrete

The detection probability C_{ij} was evaluated by an adjoint transport calculation with PARTISN5.97 [7] using the two group cross-section. As the adjoint sources, detection cross-sections $\Sigma_{d,1}$ and $\Sigma_{d,2}$ were located at detector regions ($i = 1,2$). Then, C_{ij} due to point-source ($j = 1, 2, 3$) is evaluated by Eq. (32) using the adjoint neutron flux $\phi^{\dagger}_{g,i}$ at the point of neutron source (r_j, z_j):

$$C_{ij} = \sum_{g=1}^{NG} \chi_g \phi^{\dagger}_{g,i}(r_j, z_j) = \phi^{\dagger}_{1,i}(r_j, z_j), \qquad (32)$$

where $\chi_1 = 1, \chi_2 = 0$. Only $\phi^{\dagger}_{1,i}$ were used because all neutrons released from sources are fast neutron in this calculation. Equation (32) is a discrete representation of Eq. (31).

In practical applications, y is the "measured value". However in this study, y were numerically calculated using C_{ij} and virtual true values of $A_{true,j}$, i.e. the following calculated value was regarded as the virtual measured value.

$$y_i = \sum_{j=1}^{J} C_{ij} A_{true,j}. \qquad (33)$$

It is noted that the statistical uncertainties of measured value y were neglected in this calculation. Since the relative uncertainty of neutron count can be reduced by increasing the measured count, we assume that this simplification does not significantly affect the validity of this verification.

The estimation of the ML-EM method is carried out for the following three initial distributions:
Case 1: Without spatial distribution (uniform distribution) ($A_1^{k=0}: A_2^{k=0}: A_3^{k=0} = 1:1:1$)
Case 2: With spatial distribution ($A_1^{k=0}: A_2^{k=0}: A_3^{k=0} = 3:2:1$)
Case 3: The estimation result of MPMI method ($A_1^{k=0} = A_1^{MPMI}, A_2^{k=0} = A_2^{MPMI}, A_3^{k=0} = A_3^{MPMI}$)

We used an in-house code to numerically solve radioactivity by both the ML-EM and the MPMI methods. We used the C++ library of Eigen for matrix operation [8] such as singular value decomposition in the MPMI method. The convergence criteria of the ML-EM method is given by Eq. (34):

$$\varepsilon = \sqrt{\sum_{j=1}^{J} \left(\frac{A_j^k}{A_j^{k-1}} - 1 \right)^2 \Big/ J} \leq 10^{-9}. \qquad (34)$$

V. RESULTS

Table III shows the numerical results of C_{ij}. In Table III, the row and vertical column correspond to the detector and source numbers, respectively.

Table III Numerical results of C_{ij} obtained by an adjoint transport calculation

		j: source		
		j=1	j=2	j=3
i: detector	i=1	2.63E-08	2.91E-08	2.17E-08
	i=2	1.34E-08	2.29E-08	3.63E-08

In this calculation condition, the variation of detection probabilities is not very large because distances among detectors and point-sources are similar. Since the distances between the detector of $i = 1$ and the point-source of $j = 1$ or 2 are approximately the same, C_{11} is nearly equal to C_{12} although C_{12} is slightly larger due to scattering in concrete. The trend of $C_{23} > C_{22} > C_{21}$ are observed since the detector of $i = 2$ is located at higher level than those of point-sources.

Figure 4 shows the estimated values of neutron emission rate at each point-source obtained by the ML-EM and the MPMI methods.

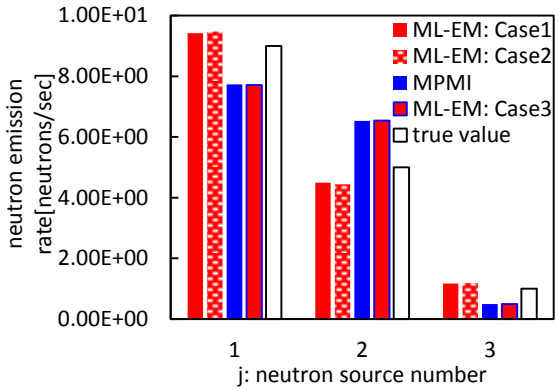

Fig. 4 Estimated value of neutron emission rate

The magnitude of the estimated value of neutron emission rate is almost the same as that of true value. The overall spatial distribution of estimated values fairly reproduce the true values. In general, the ML-EM method shows better agreement with the true values. We adopted the ML-EM and the MPMI methods, however the difference between the estimated values by both methods is not very large in this simple problem, although estimated values of the ML-EM and the MPMI methods are obtained by different procedures, i.e. the ML-EM method estimates the value whose likelihood is maximum; the MPMI method solve the minimum L2-norm solution. It was expected that the MPMI method underestimates radioactivity because it utilizes constraints of minimum L2-norm, however such a tendency is not observed in this simple calculation. It is noted that we cannot discuss the characteristic of each solution method only based on the result of this calculation; further investigation is necessary.

Since the estimation of Case 1 and Case 2 are different from Case 3, it can be found that there is the dependence on the initial distribution of the estimation in the ML-EM method. The present result suggest that there are several quasi-optimum solutions for ML-EM method. Calculation starting from initial distribution of Cases 1 and 2 reach a quasi-optimum solution and that of Case 3 reached another quasi-optimum solution.

Variation of ε expressed by Eq. (7) is shown in Fig. 5.

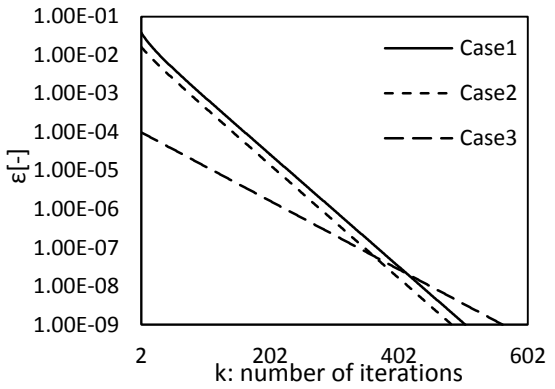

Fig. 5 Exponential decreasing of residual ε in the ML-EM method

It is fast convergence to finish with k of 10^2-order against the small convergence criteria: 10^{-9}. The convergence of methods like ML-EM had been studied [9,10] and the ML-EM method can be regarded as having a certain convergence property. However, such fast convergence cannot be guaranteed when factors such as the uncertainty of neutron count exist.

In all cases, ε shows a clear trend that the decreasing rate (the gradient) in one update is constant. Therefore, we conclude that it is appropriate to adopt the residual of Eq. (34) as convergence criteria. The decreasing rates of ε of Cases 1 and 2 are almost equal and the absolute value of ε is slightly smaller in Case 2. The latter can be understood from that Case 2 used the initial distribution closer to the true distribution than Case 1. The former trend suggests that the change of the initial distribution in the range not satisfying Eq. (10) does not have a large influence. In Case 3, the decreasing rate of ε is smaller than Case 1 and Case 2. This is presumed to reflect that the estimated value of MPMI method has little room for improvement.

VI. SUMMARY

We investigated fundamental performance of inverse estimation methods estimating radioactive source in order to contribute to the spatial distribution estimation of fuel debris which is necessary for 1F decommissioning. Actual spatial distribution of neutron emission rate is continuous, but it can be approximated by a large number of point-sources through discretization. Once discretized, estimation of spatial distribution can be cast into estimation of intensity of each point source.

Adopted calculation techniques were the ML-EM and the MPMI methods. The calculation geometry of this study was a simple model which consists of annular concrete shielding. Two group macroscopic cross-section of concrete was evaluated using SCALE6.2.1/NEWT before neutron transport calculation at the target system. Detection probability was calculated using the adjoint neutron flux. Estimated values of neutron emission rate by both methods reasonably reproduce the true values. From these results, it is concluded that both the ML-EM and the MPMI methods can be used for inverse estimation of radioactivity source.

In this preliminary study, we did not evaluate uncertainty although there are many factors of uncertainty in actual situations, e.g. detection cross-section, composition of fuel debris or shielding material, thickness of shielding and so on. Statistical uncertainty of radiation counts could become a major factor of uncertainty in the case of low count rates. In addition, the calculation model and condition of this study are considerably simplified in comparison with the actual 1F situation. Thus, further investigations are necessary to establish an uncertainty quantification method and to apply the ML-EM and the MPMI methods to more realistic calculation models and conditions.

In the ML-EM method, the estimated value was almost equal between the case where the initial distribution was uniform and the case where the initial distribution was close to the true trend. However, then estimation result by the MPMI method is used in the ML-EM method, another distribution is estimated. This results suggest that the result by the ML-EM method would show quasi-optimum solution, thus choice of initial distribution is important.

Since the residual of ML-EM method during iteration (ε) showed the clear exponential decreasing trend, use of the relative difference expressed by Eq. (34) for the convergence criteria of the ML-EM method is appropriate. In addition, the ML-EM method was found to have good convergence when the condition is simple.

NOMENCLATURE

A : radioactivity of each radioactive source
y : radiation count of each detector
C_{ij} : detection probability of radiation at detector (i) emitted from radiation source (j)
i : detector number (from 1 to I)
j : radioactive source number (from 1 to J)
k : number of iterations in ML-EM method
U : I-th order orthogonal matrix
V : J-th order orthogonal matrix
σ : singular value
diag: diagonal matrix composed of its argument
r : radial position in cylindrical geometry
z : height in cylindrical geometry
E : neutron kinetic energy
$\vec{\Omega}$: neutron flight direction
S : external neutron source
ψ : angular neutron flux
ψ^+ : adjoint angular neutron flux
Σ_d : macroscopic detection cross-section
χ : energy spectrum of fission neutron
δ : delta function
$\phi^\dagger$: adjoint neutron flux
ε : residual of the ML-EM method

REFERENCES

1. HIROKI TAKEZAWA, TORU OBARA, "Passive measure for preventing recriticality of fuel debris dust for defueling at Fukushima Daiichi nuclear power station," *J. Nucl. Sci. Technol.*, **53**, pp. 1960-1967 (2016). [in print]
2. JUNICHI KATAKURA, KEISUKE OKUMURA, KANGSOO KIM, "Technology Development to Evaluate Dose Rate Distribution and Search for Fuel Debris Submerged in water for Decommissioning of Fukushima Daiichi Nuclear Power Station (1) Objective and Research Plan," Proc. 2016 Fall Meeting of the Atomic Energy Society of Japan, 2C16, Kurume City Plaza, Japan, Sep. 7-9 2016, (2016). [CD-ROM] (in Japanese).
3. ARTUR SLOMSKI *et al.*, "3D PET image reconstruction based on Maximum Likelihood Estimation Method," Jagiellonian University (2015).
4. Lucas Parra, Harrison H. Barrett, "List mode likelihood: EM algorithm and image quality estimation demonstrated on 2D PET," *IEEE Trans. Med. Imag.*, **17**, pp. 228-235 (1998).
5. DAN GABRIEL CAUCI, "Handbook of Nuclear Engineering Nuclear Engineering Fundamentals VOL.1," Springer, pp.495-497 (2010), ISBN: 978-0-387-98130-7.
6. B.T. REARDEN, M.A. JESSEE, "SCALE Code System," ORNL/TM-2005/39 Version 6.2.1, Oak Ridge National Laboratory (2016).
7. R.E. ALCOUFFE, R.S. BAKER, J.A. DAHL, et al., "PARTISN: A Time-Dependent, Parallel Neutral Particle Transport Code System," LA-UR-05-3925, Los Alamos National Laboratory (2005).
8. "Eigen," http://eigen.tuxfamily.org/dox/, Doxygen (2016).
9. T. YOKOI *et al.*, "Implementation and Performance Evaluation of Iterative Reconstruction Algorithms in SPECT: A Simulation Study Using EGS4," Proc. Second International Workshop on EGS, Tsukuba, Japan, Aug. 8-12, 2000, pp. 224-234 (2000).
10. S. IWASAKI, "A new approach for unfolding PHA problems based only on the Bayes' Theorem," Proc. 9th International Symposium on Reactor Dosimetry, Prague, Czech Republic, Sep. 2-6, 1996, pp. 245-252 (1998).